Journal of Solid State Chemistry 181 (2008) 1701–1706

Contents lists available at ScienceDirect

Journal of Solid State Chemistry

journal homepage: www.elsevier.com/locate/jssc

The synthesis and characterization of new $[(BiSe)_{1.10}]_m[NbSe_2]_n$, $[(PbSe)_{1.10}]_m[NbSe_2]_n$, $[(CeSe)_{1.14}]_m[NbSe_2]_n$ and $[(PbSe)_{1.12}]_m[TaSe_2]_n$ misfit layered compounds ☆

Colby Heideman [a], Ngoc Nyugen [a], Jonathan Hanni [a], Qiyin Lin [a], Scott Duncombe [a], David C. Johnson [a,*], Paul Zschack [b]

[a] Department of Chemistry, University of Oregon, 373 Klamath Hall, Eugene, OR 97403, USA
[b] Advanced Photon Source, Argonne National Laboratory, 9700 S. Cass Avenue, Argonne, IL 60439, USA

ARTICLE INFO

Article history:
Received 25 March 2008
Received in revised form
3 June 2008
Accepted 3 June 2008
Available online 13 June 2008

Keywords:
Misfit layered compounds
Incommensurate structure
Layered compounds
Nanostructure

ABSTRACT

Fifty-three new misfit layered compounds within the $[(BiSe)_{1.10}]_m[NbSe_2]_n$, $[(PbSe)_{1.10}]_m[NbSe_2]_n$, $[(CeSe)_{1.14}]_m[NbSe_2]_n$, and $[(PbSe)_{1.12}]_m[TaSe_2]_n$ families of compounds were successfully synthesized. This is the first report of compounds with n and m larger than 3, as self-assembly from designed precursors allows compounds with particular n and m values to be selectively prepared. The compounds form as crystallographically aligned films, with the c-axis perpendicular to the substrate. The compounds are well ordered along the c-axis and in the ab plane, with shorter coherence lengths between the constituent layers. All 18 compounds that were measured were found to be metallic.

1. Introduction

Layered compounds have unusual physical properties, such as two-dimensional magnetism and charge density waves [1,2], can undergo low-temperature chemical transformations such as intercalation and have open coordination sites at their edges that make them useful as catalysts [3,4]. These properties have resulted in layered compounds being used commercially as lubricants, catalysts, and as cathodes in lithium batteries and has fueled continuing investigations aimed at enhancing these physical phenomena. The unusual properties have also driven synthetic efforts aimed at creating new layered compounds [5].

The misfit layered compounds are a structurally interesting subgroup of layered materials, consisting of interpenetrating transition metal dichalcogenide and distorted rock salt crystal structures with matching crystal parameters in the b and c dimensions, but an incommensurate or "mismatched" a lattice parameter [6]. Somewhat surprisingly, heating a stoichiometric combination of the elements in a sealed tube results in the formation of these compounds and single crystals can be grown by chemical transport reactions, suggesting that these compounds are thermodynamically stable. The misfit layered compounds have the general chemical formula $[(MX)_{1+x}]_m[TX_2]_n$, where approximately 90 compounds with $X = S$ and Se, $M =$ Sn, Pb, Sb, Bi, and rare earth metals, and $T =$ Ti, V, Cr, Nb and Ta have been previously reported [7,8]. The "misfit" in these compounds is given by x, which ranges from 0.07 to 0.28 in the compounds reported to date. The larger the positive value of x, the greater the atomic density of the planes in the rock salt layers relative to the dichalcogenide layers. Single-crystal diffraction data from a commensurate misfit layered compound confirm this relationship [9]. Because of differing thermal expansion coefficients for the constituent layers, the value of x can be a function of temperature. m and n represent the number of bilayers in the rock salt structure and the number of X–T–X planes in the unit cell, respectively. While any number of repeats in both subsystems should be feasible (i.e. any n and m value), the challenge is finding synthetic techniques appropriate for accessing the range of potential stable members of each family of compounds. To date, n is most commonly found to be 1 or 2, with only one or two examples known where n is 3 [10]. m has been limited to values of 1, 1.5, and 2 [11,12].

The structural incoherence between components in misfit layered compounds provides opportunities to interleave many

☆ Using layered precursors targeting specific compounds, 53 misfit layered compounds have been synthesized within the $[(BiSe)_{1.10}]_m[NbSe_2]_n$, $[(PbSe)_{1.10}]_m[NbSe_2]_n$, $[(CeSe)_{1.14}]_m[NbSe_2]_n$, and $[(PbSe)_{1.12}]_m[TaSe_2]_n$ families. These compounds show well ordered stacking along the c-axis, with large domain sizes along the c-axis and within the ab plane, relative to the shorter coherence lengths observed between constituent layers.

* Corresponding author.
E-mail address: davej@uoregon.edu (D.C. Johnson).

0022-4596/$ - see front matter © 2008 Elsevier Inc. All rights reserved.
doi:10.1016/j.jssc.2008.06.017

potential constituents to tailor physical properties, including more complex layered arrangements containing three or more components, without the constraints imposed by epitaxy. This potential, however, has been limited by the lack of a general synthetic approach with the potential to control the layered arrangement. In this paper we demonstrate that extended families of misfit layered compounds can be synthesized by depositing appropriate precursors that self-assemble into targeted $[(MX)_{1+x}]_m[TX_2]_n$ compounds. n and m can be systematically varied by adjusting the structure of the precursor. We show that we can use this approach to make $[(BiSe)_{1.10}]_1[NbSe_2]_1$, which has been previously synthesized and characterized by Wiegers et al. [13]. By varying the number of Bi/Se or Nb/Se layers deposited, we show that we can systematically prepare new compounds in this system with desired n and m values. We demonstrate that this is a general synthetic strategy by preparing new compounds in the $[(PbSe)_{1+x}]_m[NbSe_2]_n$, $[(PbSe)_{1+x}]_m[TaSe_2]_n$, and $[(CeSe)_{1+x}]_m[NbSe_2]_n$ misfit layered families. The self-assembly mechanism, structure, and electrical properties of these materials are presented.

2. Experimental

2.1. Sample preparation

Multilayer elemental precursors were deposited in a cryo-pumped high vacuum ($<5\times10^{-7}$ Torr) deposition chamber. A Thermioncs electron beam gun was used to evaporate most of the metals used while custom built effusion cells were used to evaporate selenium and the more volatile metals. Within each effusion cell a boron nitride crucible contained the element to be deposited. For all of the sources, the measured rate was determined from quartz microbalances (QMB) placed 10 in above each evaporation source. Silicon substrates were placed 12 in above each source and were coated with polymethylmethacrylate, which could be dissolved later for removal of the deposited film. To this uncoated pieces of polished silicon were attached for X-ray reflectivity (XRR) and X-ray diffraction (XRD) studies. A masked quartz substrate was also attached to create a cross pattern for van der Pauw resistivity measurements. All measured rates for metals were determined at a 64% tooling ratio while a 70% tooling ratio was used for Se. Actual deposition thicknesses were determined experimentally as reported in the subsequent section. Pneumatic shutters, timed with a personal computer, were used to control the sequence of sources deposited on the substrate, with the time the shutter remains opened controlling the thickness of each layer. For the effusion cell sources a time-averaged rate was assumed to be constant during the experimental run. For electron beam gun deposition, a feedback loop from the QMB controlled the power delivered to the gun.

2.2. X-ray reflectrometry and X-ray diffraction

XRR was used to determine thicknesses of the layered precursors and was used as a probe to follow changes in the structure of the precursor with annealing. The XRR data were analyzed using the Bede REFS software package which uses a fitting algorithm based on a first principles calculation [14]. Thickness, density, and roughness parameters for the film are refined. XRD was also used in the structure determination of the final product after annealing in an N_2 environment (<0.5 ppm oxygen). Rocking curve data were collected during the various stages of formation to indicate the degree of crystallographic alignment of the evolving crystal structure with the substrate. These studies were performed on a Bruker D8 Discover X-ray diffractometer, which used a fixed Cu $K\alpha$ (1.54 Å) radiation source, while the sample and detector were moved to achieve the desired diffraction geometries.

2.3. Electron probe microanalysis

Film compositions were determined on a Cameka SX-50 electron microprobe. Intensities were collected for silicon and oxygen in addition to the elements present in the film. Accelerating voltages of 10, 15, and 20 keV were used. The raw intensities were corrected using procedures previously described by Donovan et al. [15]. Modeling the data using StrataGEM, a thin film software program that calculates the relative signal expected from the film and the substrate as a function of accelerating voltage, yields the composition of the films [16].

2.4. Electrical measurements

Resistivity measurements were conducted using the van der Pauw method [17]. A cross was deposited using a shadow mask with arms approximately 1 cm in length and 2 mm in width onto insulating glass substrates. A Keithley 220 programmable current source provided a variable dc current and the voltage drop across the sample was measured on a Keithley 196 DMM. A Keithley 706 scanner equipped with a 7052 matrix card was used to sample all eight lead combinations which yielded the sheet resistance. Electrical contacts were made using pressure contacts directly to the arms of the film, providing ohmic contact as determined by linear IV curves. Power dissipation through the samples was monitored to prevent sample heating.

The Seebeck coefficient was measured by creating a temperature grading across the film by cooling one end with a Peltier cooler. The temperature gradient was determined using type T copper/constantan thermocouples. The voltage was measured across both the copper and constantan leads of the thermocouples. The Seebeck coefficient was determined from the slope of the voltage plotted against the temperature gradient. The slope was corrected for the Seebeck coefficients of copper and constantan by subtracting the Seebeck coefficients of these materials from the measured slope. After this correction, measurement voltages measured across copper and constantan were in agreement within 1 μV.

Room temperature measurements were performed in open atmosphere. Variable temperature measurements were made in a cryostat under vacuum with pressures below 1×10^{-5} Torr.

3. Results and discussion

The synthesis approach, which we used to prepare the targeted misfit layered compounds, requires the deposition of precursors containing layers with compositions close to that of each desired constituent and that the thickness of each layer contains the absolute amount of material required to form the desired thickness of the constituent as shown in Fig. 1. We chose to calibrate the thicknesses of the deposited layers to obtain a single Se–T–Se dichalcogenide layer and a bilayer of the constituent rock salt layer. Once the calibration of the sources to form $[(BiSe)_{1.10}]_1[NbSe_2]_1$ was accomplished, other members of this family of compounds were prepared by repeatedly depositing m layers of Bi/Se and n layers of Nb/Se to form $[(BiSe)_{1.10}]_m[NbSe_2]_n$. The subsequent calibration to prepare the other targeted systems, $[(CeSe)_{1.14}]_m[NbSe_2]_n$, $[(PbSe)_{1.10}]_m[NbSe_2]_n$, and $[(PbSe)_{1.12}]_m[TaSe_2]_n$

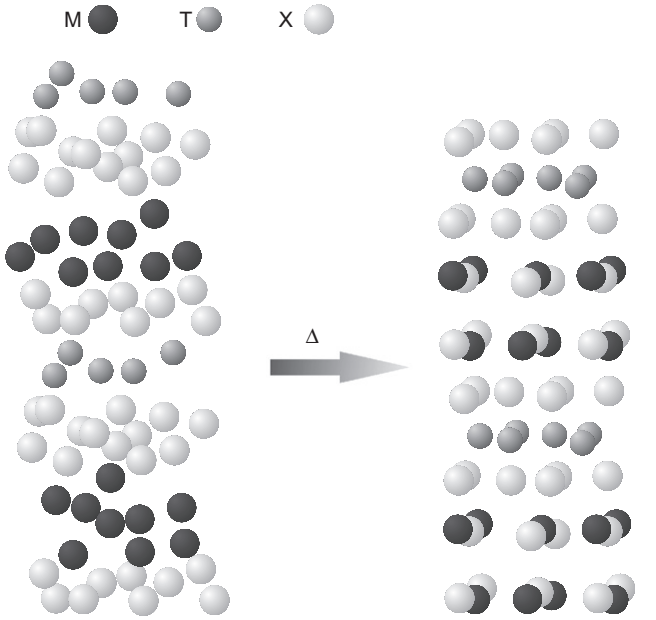

Fig. 1. Calibrating the deposition requires that the right composition and absolute number of atoms be deposited. The short diffusion distances allow low annealing temperatures enabling the retention of metastable products.

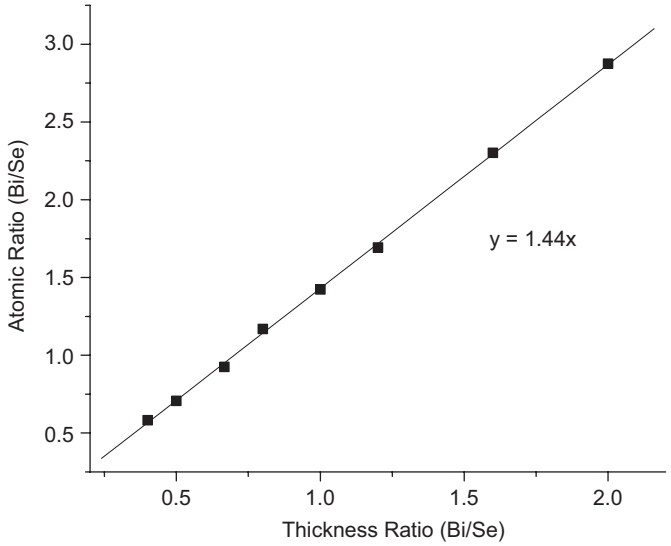

Fig. 2. Atomic ratio (from EPMA) plotted against the ratio of quartz crystal balance thickness ratio (time multiplied by deposition rate) for the Bi:Se system. A thickness ratio of 1:1.43 Bi:Se yields the desired 1:1 atomic ratio to form a BiSe rock salt layer.

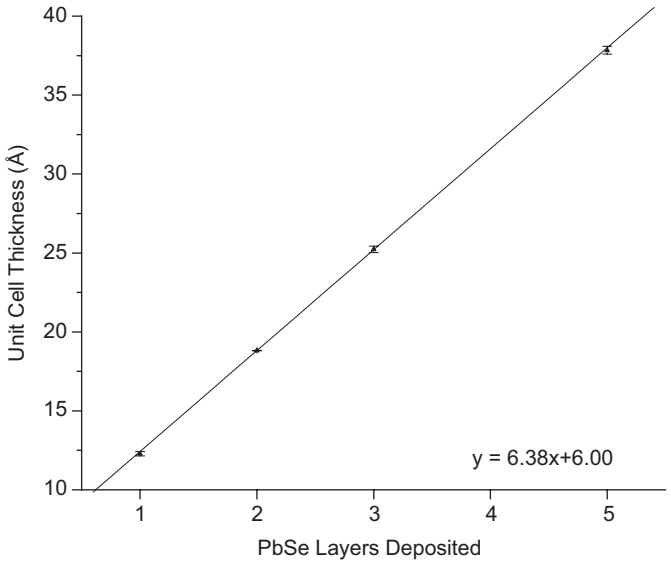

Fig. 3. Change in binary thickness within the multilayer as the number of PbSe deposition layers between $NbSe_2$ deposition layers is increased.

is considerably easier, as only one pair of elements for the new component needs to be optimized.

The calibration procedure entails determining the length of time the shutter over each elemental source is required to remain open to deposit the correct absolute amount of each element to form a single Se–*T*–Se dichalcogenide layer and a single *M*–Se rock salt bilayer. To accomplish this, the relationship between the ratio of deposition times and the resulting composition of the film is determined for each pair of elements separately. Alternating layers of the metal and chalcogen were repeatedly deposited, creating a series of samples of different compositions by holding the Se deposition time constant while increasing the metal deposition time. The resulting atomic ratio of metal to selenium was determined using electron probe microanalysis. A plot, shown in Fig. 2 using data obtained on the bismuth selenium calibration, determines the deposition parameters required to obtain the desired 1:1 composition. Scaling the deposition times for each source by a constant factor allows the thickness of a binary layer to be varied while maintaining the desired composition. XRR measurements of the films yield the actual thickness of each *M*/Se bilayer deposited, allowing the deposition parameters required to deposit approximately one unit cell worth of material to be determined.

To further refine the deposition parameters, several series of films are deposited (varying n while holding m constant, then varying m holding n constant) to optimize the absolute amount of each constituent required to form the desired Se–*M*–Se and rock salt layers. To illustrate this procedure, Fig. 3 contains a graph of the measured thickness versus m of a sequence of four $[(Pb{:}Se)_m(Nb{:}Se)_n]_z$ films where m was varied from one to five while n was held constant at one. The slope of the measured multilayer thickness as a function m corresponds to the thickness of the PbSe component of the multilayer, and the intercept to the $NbSe_2$ component. For the graph in Fig. 3, the slope indicates that the Pb/Se was thicker than desired (6.4 Å compared to a calculated thickness of 6.17 Å for the crystallized rock salt layer) while the thickness of the Nb/Se layer is close to the thickness required (6.0 Å compared to 6.32 Å calculated for the thickness of each $NbSe_2$ layer). This experiment was repeated until the parameters obtained for each constituent was within 2 percent of the targeted thickness.

Electron probe microanalysis was used to determine the ratios of the cations, and to ensure that the chalcogen content was appropriate (typically a slight excess of chalcogen is found to promote crystal growth, yielding superior diffraction patterns). An estimated misfit between the constituents is obtained from the lattice parameters of the binary components. For the, $[(PbSe)_{1+x}]_m[NbSe_2]_n$ family of compounds, this calculation yields a value of 0.07 for x, compared to a range between 0.10 and 0.14 reported in the literature for $[(PbSe)_{1+x}]_1[NbSe_2]_1$. The microprobe data for the samples used to generate Fig. 3 showed that the ratio of Pb:Nb was slightly larger than desired, at 1.3, confirming that the lead layers were too thick. When the layer thicknesses have been calibrated, the compositions determined from electron microprobe data agree with values calculated using model structures to within a percent or 2.

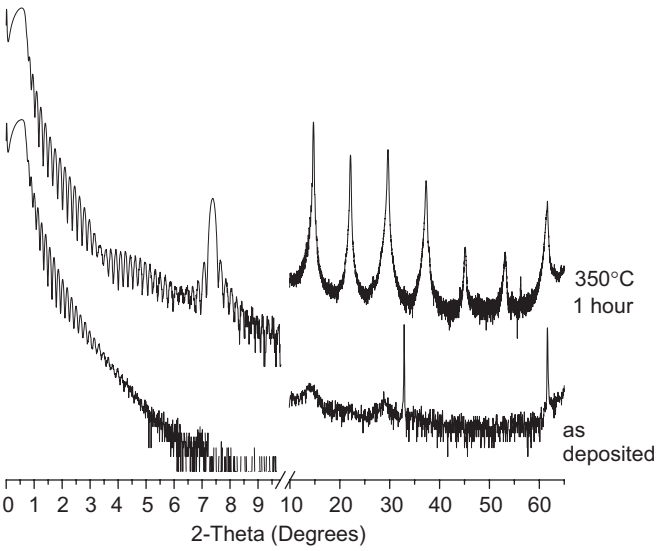

Fig. 4. Low angle reflectometry and diffraction patterns of the designed precursor film and the post-annealing self-assembled product.

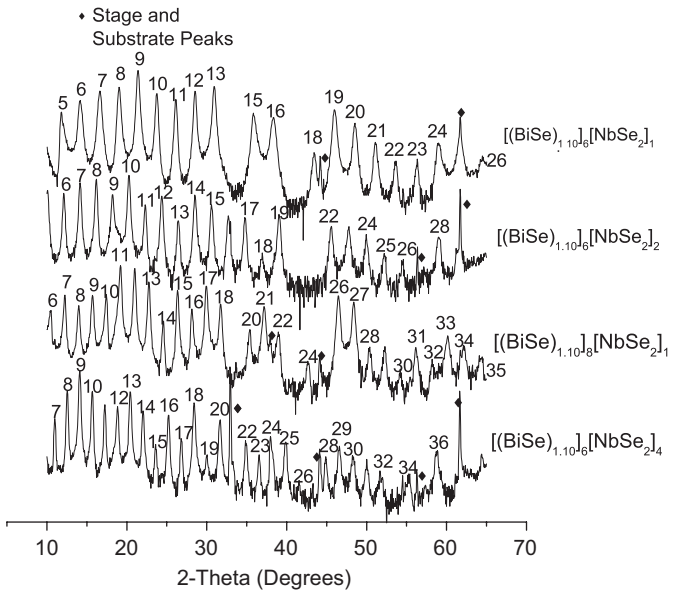

Fig. 5. Diffraction patterns for four new misfit layered compounds in the $[(BiSe)_{1.10}]_n[NbSe_2]_m$ family.

The diffraction patterns of the as-deposited films reflect their layered structure. The low angle diffraction pattern at the bottom of Fig. 4 is that of the Nb/Se:Bi/Se sample designed to form the $n = m = 1$ compound $[(BiSe)_{1.10}]_1[NbSe_2]_1$. As deposited, Kiessig fringes are observed out to 4.15° $2-\theta$ indicating a roughness around 15 Å from modeling studies. The diffraction maxima at 6.93° $2-\theta$ is the first Bragg reflection resulting from the regular layering in the as-deposited film. At higher angles, weak, broad diffraction peaks indicate small crystallites of the 1:1 compound that have begun to self-assemble even in the as-deposited film. As the sample is annealed, the film becomes significantly smoother, with fringing extending out to 22.79° $2-\theta$ and diffraction peaks corresponding to the $0\,0\,l$ lattice planes grow in as the superstructure self-assembles. The slow growth of the diffraction maxima with time and temperature indicates slow ripening of crystallites rather than a nucleation followed by a rapid crystallization. This is supported by differential scanning calorimetry, which shows a broad exotherm that generally starts around 250 °C and ends by 400 °C for these compounds, with a maximum around 350 °C. Diffraction data collected as a function of temperature show the largest increase in the intensity of the diffraction pattern of the phase formed is observed between 300 and 400 °C. As the sample is annealed, the width of the rocking curve also narrows from 11.3° to 2.7° θ as the preferred alignment of the crystallites increases. After annealing at 350 °C, the diffraction pattern contains all of the expected $0\,0\,l$ diffraction maxima. Diffraction data collected in the a–b plane yields a value of 1.10 for the misfit between the constituents.

Once the deposition sequence is optimized to an extent that the compound $[(BiSe)_{1.10}]_1[NbSe_2]_1$ self-assembles, other compounds in this family are made by varying the number of repetitions in the depositions sequence and annealing the films. Fig. 5 contains the diffraction patterns of several new members of this family of compounds. Table 1 shows the samples prepared in this family, with unit cells as large as 103.50 Å prepared. Plotting the size of the unit cell of the annealed compounds against the number of layers deposited shows a linear increase in the size of the unit cell, with a slope of 6.32 Å when increasing the number of Nb:Se layers deposited, indicating that an individual layer of $NbSe_2$ forms from each deposited layer. In theory, it should be possible to make every $[(BiSe)_{1.10}]_m[NbSe_2]_n$ compound, although experimentally, some have proved challenging. For example, the

Table 1
Summary of samples made in the $[(BiSe)_{1.10}]_n[NbSe_2]_m$ family

BiSe bilayers	$NbSe_2$ layers	Unit cell thickness (Å)
1	1	12.047(8)
1	2	18.5(2)
1	3	25.1(3)
1	4	30.9(2)
1	5	37.37(5)
3	1	22.11(3)
3	3	35.07(3)
4	1	27.75(4)
4	2	34.08(9)
5	3	46.2(5)
5	5	59.1(4)
6	1	37.5(1)
6	1	37.33(3)
6	2	43.79(4)
6	3	50.09(8)
6	4	56.73(5)
6	5	63.0(3)
7	4	62.0(2)
8	1	50.73(7)
8	4	66.21(8)
8	4	66.2(2)
9	3	69.6(3)
10	4	76.4(3)
11	3	78.9(2)
11	4	82.5(2)
13	4	90.6(2)
14	4	99.2(2)
15	4	103.5(4)

compounds $[(BiSe)_{1.10}]_2[NbSe_2]_1$ and $[(BiSe)_{1.10}]_3[NbSe_2]_1$ have only been made as part of mixed phase films while increasing the thickness of the rock salt block further results in the successful synthesis of single-phase compounds with m ranging from 4 to 15.

This synthetic strategy permits the synthesis of many new misfit layered compounds. Table 2 contains a summary of information on the as-deposited films and of the new compounds prepared in the $[(PbSe)_{1.10}]_m[NbSe_2]_n$, and $[(PbSe)_{1.12}]_m[TaSe_2]_n$ families of compounds. We have also been successful synthesizing entirely new families of misfit layered compounds. Fig. 6 shows the diffraction patterns of four new compounds from the

Table 2
Lattice parameters from 21 misfit layered compounds self-assembled from precursors targeting each structure

m	*n*	Unit cell thickness (Å)
$[(CeSe)_{1.14}]_m[NbSe_2]_n$		
2.5	4	39.5(1)
2.5	6	52.3(1)
2.5	8	65.2(2)
2.5	10	77.9(1)
1	8	56.5(1)
2.5	8	65.1(4)
4	8	73.5(2)
1	4	31.5(6)
2.5	4	39.6(1)
4	4	48.0(2)
$[(PbSe)_{1.12}]_m[TaSe_2]_n$		
1	1	12.49(1)
1	2	18.95(3)
1	5	38.13(6)
2	1	18.61(1)
2	2	25.05(5)
2	3	31.45(5)
2	4	37.80(6)
3	1	24.73(7)
3	2	31.50(8)
3	3	37.51(5)
4	4	49.8(2)
$[(PbSe)_{1.10}]_m[NbSe_2]_n$		
1	1	12.439(7)
1	2	18.82(2)
1	3	25.2(2)
1	5	37.8(2)
2	1	18.57(4)
3	1	24.7(3)
2	2	24.9(1)

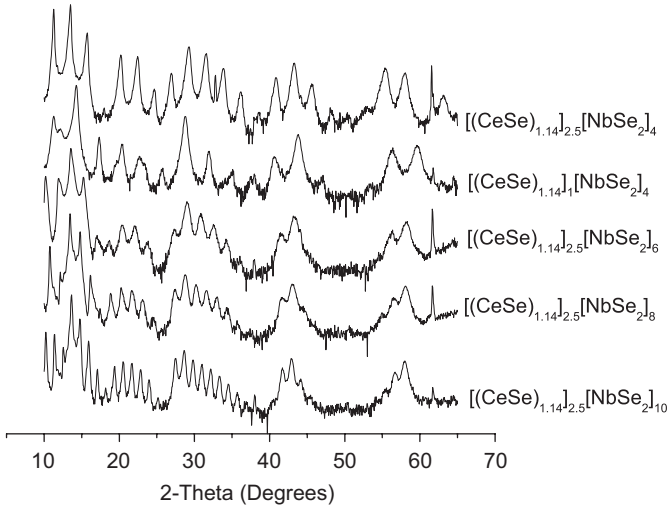

Fig. 6. Several diffraction patterns from new materials from the $[(CeSe)_{1.14}]_m[NbSe_2]_n$ family of compounds.

$[(CeSe)_{1.14}]_m[NbSe_2]_n$ misfit layered compound family. An increase of 5.66 Å is found in the *c* lattice parameter when *m* is varied while holding *n* constant and an increase of 6.41 Å is observed while *n* is varied and *m* is constant. The value per $NbSe_2$ sub unit is very similar to that observed in the literature for other misfit compounds as well as the other families of $NbSe_2$ containing misfit compounds presented in this paper. Fig. 7 shows a cross section TEM image, revealing the layered structure with areas of high strain resulting from the misfit between layers and the relatively small *a*–*b* plane grain sizes for the constituent layers.

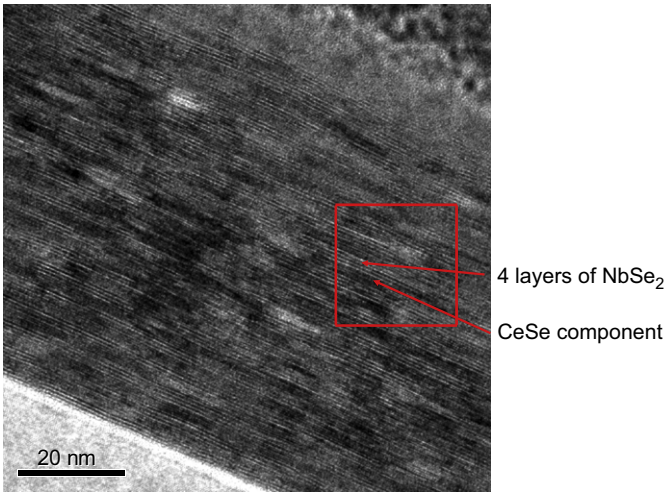

Fig. 7. TEM image of $[(CeSe)_{1.14}]_m[NbSe_2]_4$. The CeSe component appears stressed as evidenced by the dark regions appearing in the image.

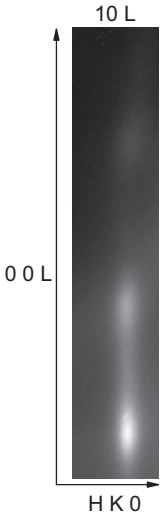

Fig. 8. Area diffraction image around the 10*l* family of diffraction peaks for $[(BiSe)_{1.10}]_1[NbSe_2]_1$. The broad peak width along 00*l* relative to *hk*0 for these mixed reflections indicates short-range order between constituent layers.

Plotting the *c*-lattice parameters for each family as a function of *n* and *m* reveals a regular change in structure both within and between families of compounds. The increase in *c*-lattice parameter per $NbSe_2$ layer ranges from 6.32 to 6.41 Å for the three families of $[(MSe)_{1+x}]_m[NbSe_2]_n$ compounds prepared. This is close to the value of 6.32 Å reported previously for $NbSe_2$ containing misfit compounds [10]. Likewise, a regular increase of 6.12–6.13 Å per PbSe bilayer is observed for the two $[(PbSe)_{1+x}]_m[TSe_2]_n$ families prepared, which agrees well with 6.12 Å reported previously for PbSe containing misfit compounds [10]. Diffraction patterns collected to reveal the in-plane structure contain diffraction maxima corresponding to the rock salt and transition metal dichalcogenide components. While the structure of the new misfit layered compounds reported here are very similar to previously made materials, they were found to have a very short structural coherence between the constituent layers as evidenced (see Fig. 8) by the width of mixed *hkl* reflections in the 00*l* direction.

Based on prior literature measurements in these families of compounds, we expected them all to be metals [18,19], with

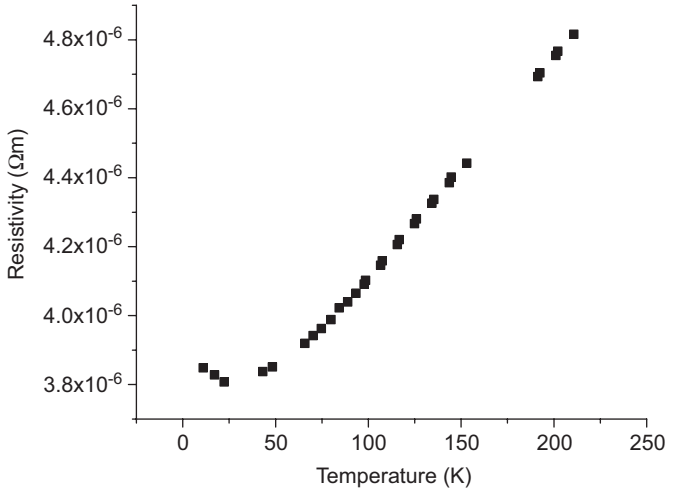

Fig. 9. Variable temperature resistivity for $[(PbSe)_{1.10}]_1[NbSe_2]_1$. Metallic behavior is observed down to around 40 K, where impurities begin to dominate the conductivity.

Table 3
In-plane electrical resistivity measurements from the family $[(PbSe)_{1.10}]_m[NbSe_2]_n$ and Seebeck coefficients from the family $[(PbSe)_{1.12}]_m[TaSe_2]_n$

Compound	Resistivity (Ω m)
$[(PbSe)_{1.10}]_1[NbSe_2]_1$	6.80E−06
$[(PbSe)_{1.10}]_1[NbSe_2]_2$	5.63E−06
$[(PbSe)_{1.10}]_1[NbSe_2]_3$	5.59E−06
$[(PbSe)_{1.10}]_2[NbSe_2]_1$	1.37E−05
$[(PbSe)_{1.10}]_3[NbSe_2]_1$	3.68E−05
$[(PbSe)_{1.10}]_2[NbSe_2]_2$	3.49E−06
Compound	**Seebeck coefficient (μV K^{-1})**
$[(PbSe)_{1.10}]_1[TaSe_2]_1$	61
$[(PbSe)_{1.10}]_1[TaSe_2]_2$	36
$[(PbSe)_{1.10}]_1[TaSe_2]_3$	25
$[(PbSe)_{1.10}]_1[TaSe_2]_4$	23

significant anisotropy. While we have yet to measure all of the compounds reported herein, initial resistivity data collected on 18 $[(PbSe)_{1.10}]_m[NbSe_2]_n$, $[(PbSe)_{1.10}]_m[NbSe_2]_n$, and $[(PbSe)_{1.12}]_m[TaSe_2]_n$ compounds discussed in this paper show that they all have metallic behavior in the *a*–*b* plane. Fig. 9 shows resistivity data collected as a function of temperature for $[(PbSe)_{1.10}]_1[NbSe_2]_1$. The resistivity data have a linear temperature dependence down to 40 K, where defects become the dominant scattering mechanism and the resistivity becomes temperature independent. Our 50 nm thick film of $[(PbSe)_{1.10}]_1[NbSe_2]_1$ has a resistivity of $6.8\times10^{-6}\,\Omega$ m which is only slightly higher than reported for the bulk material ($4.0\times10^{-6}\,\Omega$ m). In this family of compounds, the room temperature resistivity was found to be relatively independent of the number of $NbSe_2$ layers, but increased significantly as the PbSe block thickness was increased as shown in Table 3 for small *n* and *m* values. Seebeck coefficients for $[(PbSe)_{1.12}]_m[TaSe_2]_n$ range from 61 μV/K for $[(PbSe)_{1.12}]_1[TaSe_2]_1$ to 23 μV/K for $[(PbSe)_{1.12}]_1[TaSe_2]_4$ at room temperature. Further measurements aimed at quantifying the change in electrical and magnetic properties as a function of the thickness of the constituent layers are underway.

4. Conclusion

We have prepared over 50 new misfit layered compounds, $((MX)_{1+x})_m(TX_2)_n$ where M = Pb, Bi and Ce, T = Nb, Ta, using the self-assembly of designed reactants to target particular *n*, *m* compounds. *n* and *m* values as large as 15 and 10, respectively, have been prepared, but we have not probed the limit of this approach. Very regular changes in lattice parameters were observed as *n* and *m* were varied, as expected from the insertion of regular structural units. The compounds were found to be very crystalline perpendicular to the layering (i.e. along the *c*-axis) and in the *a*–*b* plane. The structural coherence between the layers was found to be smaller. All of the compounds investigated to date were metallic—in agreement with the several known members of these families reported in the literature.

References

[1] J.W. Lynn, W.H. Li, Q. Li, H.C. Ku, H.D. Yang, R.N. Shelton, Phys. Rev. B: Condens. Matter 36 (1987) 2374–2377.
[2] J.A. Wilson, F.J. Di Salvo, S. Mahajan, Adv. Phys. 24 (1975) 117–201.
[3] Y. Kanzaki, S. Ogura, O. Matsumoto, Y. Toida, Physica B+C (Amsterdam) 114 (1982) 379–383.
[4] H. Tributsch, Z. Naturforsch. A 32A (1977) 972–985.
[5] L. Cario, H. Kabbour, A. Meerschaut, Chem. Mater. 17 (2005) 234–236.
[6] A. Meerschaut, Curr. Opin. Solid State M 1 (1996) 250–259.
[7] G.A. Wiegers, A. Meerschaut, Mater. Sci. Forum 100–101 (1992) 101–172.
[8] G.A. Wiegers, Prog. Solid State Chem. 24 (1996) 1–139.
[9] Y.C. Hung, S.J. Hwu, Inorg. Chem. 32 (1993) 5427–5428.
[10] Y. Oosawa, Y. Gotoh, J. Akimoto, T. Tsunoda, M. Sohma, M. Onoda, Jpn. J. Appl. Phys. Part 2 31 (1992) 1096–1099.
[11] H. Bengel, S. Jobic, Y. Moelo, A. Lafond, J. Rouxel, D.K. Seo, M.H. Whangbo, J. Solid State Chem. 149 (2000) 370–377.
[12] L. Cario, A. Lafond, P. Palvadeau, C. Deudon, A. Meerschaut, J. Solid State Chem. 147 (1999) 58–67.
[13] V. Petricek, I. Cisarova, J.L. De Boer, W. Zhou, A. Meetsma, G.A. Wiegers, S. Van Smaalen, Acta Crystallogr. B: Struct. Sci. B 49 (1993) 258–266.
[14] M. Wormington, C. Panaccione, K.M. Matney, D.K. Bowen, Philos. Trans. R. Soc. London A 357 (1999) 2827–2848.
[15] J.J. Donovan, T.N. Tingle, J. Microsc. Soc. Am. 2 (1996) 1–7.
[16] J.L. Pouchou, F. Pichoir, Electron Probe Quant. (1991) 31–75.
[17] L.J.v.d. Pauw, Philips Tech. Rev. 20 (1958) 220–224.
[18] W.Y. Zhou, A. Meetsma, J.L. De Boer, G.A. Wiegers, Mater. Res. Bull. 27 (1992) 563–572.
[19] C. Auriel, R. Roesky, A. Meerschaut, J. Rouxel, Mater. Res. Bull. 28 (1993) 247–254.